Convective and Rainfall Properties of Tropical Cyclone Inner Cores and Rainbands from 11 Years of TRMM Data

HAIYAN JIANG

Department of Earth & Environment, Florida International University, Miami, Florida

ELLEN M. RAMIREZ

Department of Atmospheric Sciences, University of Utah, Salt Lake City, Utah

DANIEL J. CECIL

Earth System Science Center, University of Alabama in Huntsville, Huntsville, Alabama

(Manuscript received 15 December 2011, in final form 6 July 2012)

ABSTRACT

Convective and rainfall properties of tropical cyclones (TCs) are statistically quantified by using Tropical Rainfall Measuring Mission (TRMM) data from December 1997 to December 2008. A semimanual method is used to divide the TC raining area into inner core (IC), inner rainband (IB), and outer rainband (OB) regions. Precipitation features (PFs) within these regions are compared for their convective vigor and rainfall characteristics based on passive microwave, infrared, radar, and lightning properties. Strong convective signatures are generally found more often in precipitation features in the IC region, less often in the IB region, and least often in the OB region when examining features with sizes greater than 1000 km^2. However, at the very strong end of the convective spectrum, the magnitude of ice scattering signatures in OB features tends to be comparable and even stronger than that in IC features. The flash density when normalized by the raining area is about 2–3 times higher in IC features than that in OB features for all TCs except for category-1–2 hurricanes, in which the flash density is comparable for IC and OB features. The flash count per raining area in IB features is a factor of 2 (4) lower than that in OB (IC) features for all TC intensity categories on average. This confirms the bimodal radial distribution of flash density as suggested by previous studies. However, instead of a weaker maximum in the IC region and a stronger maximum in the OB region, this study finds a stronger maximum in the IC region and a weaker maximum in the OB region.

1. Introduction

Observations of tropical cyclones (TCs) are limited because they spend most of their lifetime over open oceans. The Tropical Rainfall Measuring Mission (TRMM) satellite marks the first time that TCs in all ocean basins can be viewed by a high-resolution precipitation radar from orbit. After 13 full years of successful operation, TRMM measurements from the TRMM Microwave Imager (TMI), Precipitation Radar (PR), Visible and Infrared Scanner (VIRS), and Lightning Imaging Sensor (LIS) have provided invaluable sources of data for the study of TC structure, intensity, and intensity change. The convective and precipitation structure in different regions of TCs is a fundamental and important piece of information for the TC research community. Observational and modeling studies (Schubert and Hack 1982; Hendricks et al. 2004; Kelley et al. 2004; Montgomery et al. 2006; Reasor et al. 2009; Guimond et al. 2010; Rogers 2010; Montgomery and Smith 2011; Jiang 2012) have linked deep convection with TC intensification in general and rapid intensification in particular. Satellite-based inner core areal mean rainfall and ice scattering signatures have also been linked with future TC intensity (e.g., Rao and MacArthur 1994; Cecil and Zipser 1999). Current TC simulations usually produce unrealistic storm rainfall and convective structures because of incorrect microphysics schemes. Satellite-based, long-term statistics of the convective and precipitation structure of TCs

Corresponding author address: Dr. Haiyan Jiang, Department of Earth & Environment, Florida International University, 11200 SW 8th Street, PC-342B, Miami, FL 33199.
E-mail: haiyan.jiang@fiu.edu

DOI: 10.1175/MWR-D-11-00360.1

will help TC researchers better understand the importance of convection to storm development and help modelers improve their TC simulations, therefore improving TC prediction.

It has been documented that convective systems over tropical oceans, including TCs, generally produce weaker vertical motions and have weaker convective intensity than their continental counterparts (LeMone and Zipser 1980; Jorgensen and LeMone 1989; Lucas et al. 1994). Observations of convective activity over the ocean indicate that there are sharp decreases in radar reflectivity above the melting layer (Szoke et al. 1986; Black et al. 1996; Cecil et al. 2002), modest passive microwave ice scattering signatures (Cecil and Zipser 1999, 2002), and relatively low lightning flash rates (Black et al. 1986; Samsury and Orville 1994; Molinari et al. 1999; Cecil et al. 2002; Toracinta et al. 2002). The likelihood of a precipitation feature having lightning is 40 times greater over land than over ocean (Cecil et al. 2005; Liu et al. 2011).

In contrast, Heymsfield et al. (2010) argued that many biases in measurements of convective intensity (e.g., strength of updrafts) have often been related to the field experiment, cloud penetration safety issues, the specific aircraft used for the studies, and the type of instrumentation. They studied deep convection cases over land and ocean in the tropics and subtropics using high-resolution measurements of vertical velocities in intense convection from the nadir-viewing high-altitude Earth Resources-2 (ER-2) Doppler radar (EDOP). They found that strong updrafts (between 15 and 30 m s^{-1} with a few exceeding 30 m s^{-1}) exist in all their cases and land-based storms only had slightly stronger updrafts than the oceanic and tropical cyclone convection cases. Heysmfield et al. note that most of their oceanic and tropical cyclone cases were near coasts, where satellite data suggest stronger convection than farther out over the oceans. On the other hand, their land cases do not cover the strong end of the continental spectrum.

In terms of the convective intensity in different regions of TCs, Szoke et al. (1986) found that the mean radar reflectivity profiles are similar above the freezing level for convective cells in hurricane rainbands and in general tropical oceanic rainfall systems, but the mean eyewall reflectivity profile above the freezing level shows stronger convective intensity. Jorgensen et al. (1985) and Black et al. (1996) found that inner rainbands exhibit weaker updraft magnitudes than do eyewalls. Cecil et al. (2002) and Cecil and Zipser (2002) showed that the convective cores within the eyewall region have the highest reflectivity compared with those in the inner and outer rainbands. In terms of ice scattering signatures derived from microwave observations, Cecil et al. (2002) demonstrated that the eyewall region has a higher percentage of samples with depressed 85- and 37-GHz polarization corrected brightness temperatures (PCTs; Spencer et al. 1989; Cecil et al. 2002) than both the inner rainband and outer rainband regions. However, Cecil et al. (2002) and Cecil and Zipser (2002) used only 1 yr of TRMM data including 261 overpasses of 45 hurricanes or strong tropical storms with distinguishable eyewalls. Weaker-intensity storms, that is, weak tropical storms and tropical depressions, are not included in these studies. The main purpose of this study is to quantitatively compare convective and rainfall characteristics in the inner core, inner rainband, and outer rainband regions for a large variety of TCs in different intensity stages.

A smaller lightning flash density in the inner rainband region compared to the rest of the hurricane has been found by Molinari et al. (1999) using data from the National Lightning Detection Network (NLDN) and was confirmed by Cecil et al. (2002) using TRMM LIS data and also by Abarca et al. (2011) using the World Wide Lightning Location Network (WWLLN) data. However, some opposite results have been found by Yokoyama and Takayabu (2008; using TRMM data) and DeMaria et al. (2012; using WWLLN data), who suggested that the lightning density decreases monotonically with a radius out to 500–1000 km. Molinari et al. (1999) determined that eyewall cloud-to-ground flash densities show a relatively weak maximum and that outer rainband cloud-to-ground flash densities show a relatively strong maximum. In contrast, Cecil et al. (2002) found that total (intracloud, cloud to cloud, and cloud to ground) lightning flash densities in the eyewall region and outer rainband region, normalized by the total precipitation area, are similar and 4 times greater than in the inner rainband region. Cecil et al. (2002) hypothesized that this difference might be due to deficiencies in the sample size, which could be a significant source of uncertainty in either study. Molinari et al. (1999) used the continuous coverage of NLDN for 9 Atlantic basin hurricane samples, while Cecil et al. (2002) used 1 yr of TRMM satellite data, which include 261 overpasses (snapshots) of 45 hurricanes. Another hypothesis is that the ratio of in-cloud to cloud-to-ground flashes might increase in the inner core region. Abarca et al. (2011) refuted this hypothesis by comparing the WWLLN (which measures some in-cloud flashes) and NLDN (which does not target in-cloud flashes) data. However, as a result of the very low detection efficiency of WWLLN, the question about how lightning flashes distribute in different TC regions remains unsolved.

Studies have shown that TCs contain relatively little lightning compared to tropical continental features (Toracinta et al. 2002; Cecil et al. 2002). The likelihood of a precipitation feature (PF) having lightning is 40

times greater over land than over ocean (Cecil et al. 2005; Liu et al. 2011).

As summarized in DeMaria et al. (2012), total lightning measurements are needed in TCs to provide the most information concerning the convective evolution and related intensity and structure changes. The LIS on TRMM has continued to provide total lightning measurements since 1998 (Christian et al. 1992, 1999). The lightning detection efficiency of LIS is estimated to range between about 70% during daytime and 90% at night (Boccippio et al. 2002). Although LIS only provides snapshots of lightning locations and cannot be used to study the evolution of individual storms, it can be used to provide climatologies of lightning in TCs through compositing approaches as done by Cecil et al. (2002) using 1 yr of TRMM data.

In this study, a much larger database is used to quantitatively compare convective and rainfall characteristics including lightning properties in distinct TC regions for different TC intensity categories including tropical depressions (TDs), tropical storms (TSs), and category-1–2 (CAT12) and category-3–5 (CAT35) hurricanes. The data used here include over 5000 TC overpasses of about 900 TCs during December 1997–December 2008 from the TRMM Tropical Cyclone Precipitation Feature (TCPF) database (Jiang et al. 2011). Properties to be investigated include the TRMM-derived 85- and 37-GHz PCTs, infrared (IR) 11-μm brightness temperature, rain rate, raining area, reflectivity profiles, and lightning. The TC inner core, inner rainband, and outer rainband regions are divided subjectively by using a semimanual method adapted from Cecil et al. [2002 (CZN02)]. This study is mainly a continuation of the work of CZN02, but the statistics to be presented will include and compare TCs in different intensity stages instead of only examining stronger storms as in CZN02.

2. Data and methodology

The data used in this study include observations from TRMM. The TRMM satellite was launched in November of 1997 (Simpson et al. 1988) and remains operational at the time of this writing. During August 2001 its altitude was boosted from 350 to 402 km to reduce drag and therefore increase its lifetime in orbit. The TMI has a 760-km swath width before the TRMM boost and 878-km swath width after boost. The PR has a much narrower swath width (215 km before the TRMM boost and 247 km after). Both TMI and PR swath data are used in this study to maximize the sample size and use the unique 3D observations from the radar. For a more detailed description of TRMM sensors, please refer to CZN02.

a. TC region separation methodology

The TC region categorizations used in this study follow the three distinct TC regions that were subjectively identified by CZN02 using TRMM TMI and PR observations. These categories are 1) the eyewall region, 2) the inner rainband region, and 3) the outer rainband region. The eyewall region is a quasi-circular band of precipitating clouds around the storm circulation center that slopes outward with height. In CZN02, only hurricanes or tropical storms with distinguishable eyewalls seen by the PR were included. In contrast, this study includes all intensity stages of TCs that reached the tropical storm intensity level or above at least once in their lifetime. Therefore, each individual TRMM overpass included here could be at either tropical depression, tropical storm, or hurricane stage. In the cases of low-intensity TCs without a discernible eye, and therefore no eyewall, near-center convection is included. Therefore, this category is defined as the *inner core* (IC) instead of the eyewall region in this study. The purpose of including TCs with no defined eyewalls is to allow comparisons of convective properties across the whole spectrum of storm intensity. The IC region includes complete eyewalls, incomplete or partial eyewalls, concentric eyewalls, and near-center convection for storms without an eye. Similar to CZN02, the outer boundary of IC is identified by the outer edge of the horizontal gradient of reflectivity or 85/37-GHz PCT (which indicates ice scattering). The *inner rainband* (IB) region includes banded or bloblike precipitation immediately outside of the IC boundary. It usually extends from the IC boundary outward about 100 km, and is usually bounded on the outside by a rain-free region adjacent to the outer rainband. The *outer rainband* (OB) region includes outward spiraling banded precipitation and any precipitation features associated with the cyclone located beyond about 150–200 km from the storm center. The outer boundary of the OB is determined by the farthest distance that all TC precipitation features extend, or at most 500 km from the center of the TC to the center of the precipitation feature. Storm center locations are linearly interpolated from the ''best track'' data. Please see section 2b for details about the best track data and the definition of TCPFs.

More than 12 000 TRMM overpasses of 940 TCs from December 1997 through December 2008 are subdivided into IC, IB, and OB regions (collectively referred to as TC regions) by subjectively analyzing gradient and transition zones in TMI and PR orbital data. Radial limits for each TC region are assigned with the aid of concentric circles. Each assigned radial limit is rounded to 5 km. This TC region separation procedure is partially an extension of CZN02, who hand traced TC regions for 261

TRMM-observed TC overpasses from December 1997 through December 1998. Since it is nearly impossible to hand trace about 50 times more data used in this study, the present work instead uses circles to define TC regional boundaries. Defining a TC region is not a clear-cut process, so several guidelines are employed. For example, the partial extension of asymmetric IC convection into the designated IB region is sometimes inevitable. In such instances, the IC boundary is usually extended farther out radially, which then makes the IC subject to IB contamination, and also drives up the mean IC radius. However, if the tail end of the strong IC band of convection extends far enough out so that the majority of the lightly raining IB bands would end up in the IC, then the radius of IC convection would be truncated such that the IB would be subject to IC contamination. Note that this becomes more of an issue when looking at maximum and minimum PF properties. As involved in any subjective method, errors or biases could be introduced because of the subjective procedure. However, since we used the convective structure from the horizontal fields of radar reflectivity and passive microwave ice scattering, the subjective separation of IC, IB, and OB regions can take the different storm sizes into account and is better than using a fixed radius to define these regions for all TCs.

Similar to CZN02, both the PR reflectivity and TMI 85/37-GHz ice scattering signatures are used as TC region discriminators. However, this study includes overpasses in which the PR data are not available to cover the TC inner core region because of the narrow swath of the PR. Observations beyond the PR swath increase the sample size of this study dramatically. For example, the IC region was completely captured by the TMI swath for about 56% of all the TMI TC overpasses used in this study and only 8% of all the PR TC overpasses by the PR swath. The IC region was entirely missed by the PR swath for 67% of the total PR sample, and for 28% of the total TMI sample. Therefore, two datasets are used in this study: 1) the PR swath only (to use the unique observations of the vertical profiles of radar reflectivity), and 2) the TMI swath only (to have a very large sample size). For those cases beyond the PR swath, the most useful discriminator is the 85-GHz PCT because of its sensitivity to precipitation-sized ice particles that are characteristically present in strong IC updrafts. The 37-GHz PCT images are also used to do the separation.

Figure 1 shows an example of the partition of IC, IB, and OB regions for Typhoon Namtheun (2004). This overpass is ideal because it passes directly over the TC center and the precipitation is roughly concentric. In the PR near-surface reflectivity and maximum reflectivity projection panels (Figs. 1a,b), the eyewall is a perfect ring shape around the TC center with more than 40-dBZ reflectivity in the southwest half of the ring. This ring extends to about a 40-km radius in radar images. This convection is encircled by an echo-free annulus between 40- and 60-km radii. However, in the TMI 85-GHz PCT image (Fig. 1c), the eyewall convection as indicated by a 250-K PCT contour is in half-ring shape and extends up to a 50-km radius. In the 37-GHz PCT image (Fig. 1d), the eyewall convection as indicated by a 270-K PCT contour appears as a convective blob and extends to a 60-km radius. Therefore, the IC boundary is determined as 60 km in this case to be consistent with both PR and TMI observations. The IB region consists of secondary lines of precipitation, $\geq$35-dBZ reflectivities, and depressed PCTs inward of 150 km. The OB region lies between 150 and 570 km, where deep convective cells are embedded in outward spiraling rainbands.

The mean and standard deviations of the radial extent of IC, IB, and OB regions are given in Table 1 for all 11 yr of TRMM TC overpasses used in this study. The mean extents of the IC, IB, and OB are 82, 162, and 502 km, respectively. CZN02 reported that the mean radii of their eyewall, IB, and OB regions were 50, 135, and 350 km, respectively, which are all smaller than what we determined here. The discrepancy is mainly due to the fact that CZN02's sample included only mature TCs with well-defined eyewalls, whereas this study includes all near-center convection, even for disorganized systems. Additionally, CZN02 used both PR and TMI data inside the PR swath, but this study includes all TMI data in a wider swath where radar observations may or may not be available.

b. The TRMM TCPF database

Precipitation features were defined by grouping contiguous pixels based on certain criteria as observed by TRMM (Nesbitt et al. 2000; Liu et al. 2008). A variety of different criteria are used to define PFs. For example, Nesbitt et al. (2000) selected contiguous areas with near-surface reflectivity equal or greater than 20 dBZ or 85-GHz PCT equal or less than 250 K as PFs. As mentioned above, both PR-swath-only and TMI-swath-only data are used in this study. Therefore, two types of precipitation feature definitions are used (Table 2): one in the TMI swath with 2A12 (Kummerow et al. 1996) rain rate greater than zero (TTPF) and one in the PR swath with 2A25 (Iguchi et al. 2009) rain rate greater than zero (RPFs).

The TRMM Tropical Cyclone Precipitation Feature (Jiang et al. 2011) database includes all PFs that are associated with TCs. To be qualified as a TCPF, the distance between the TC center and the PF center has to be less than 500 km. Storm center locations are linearly

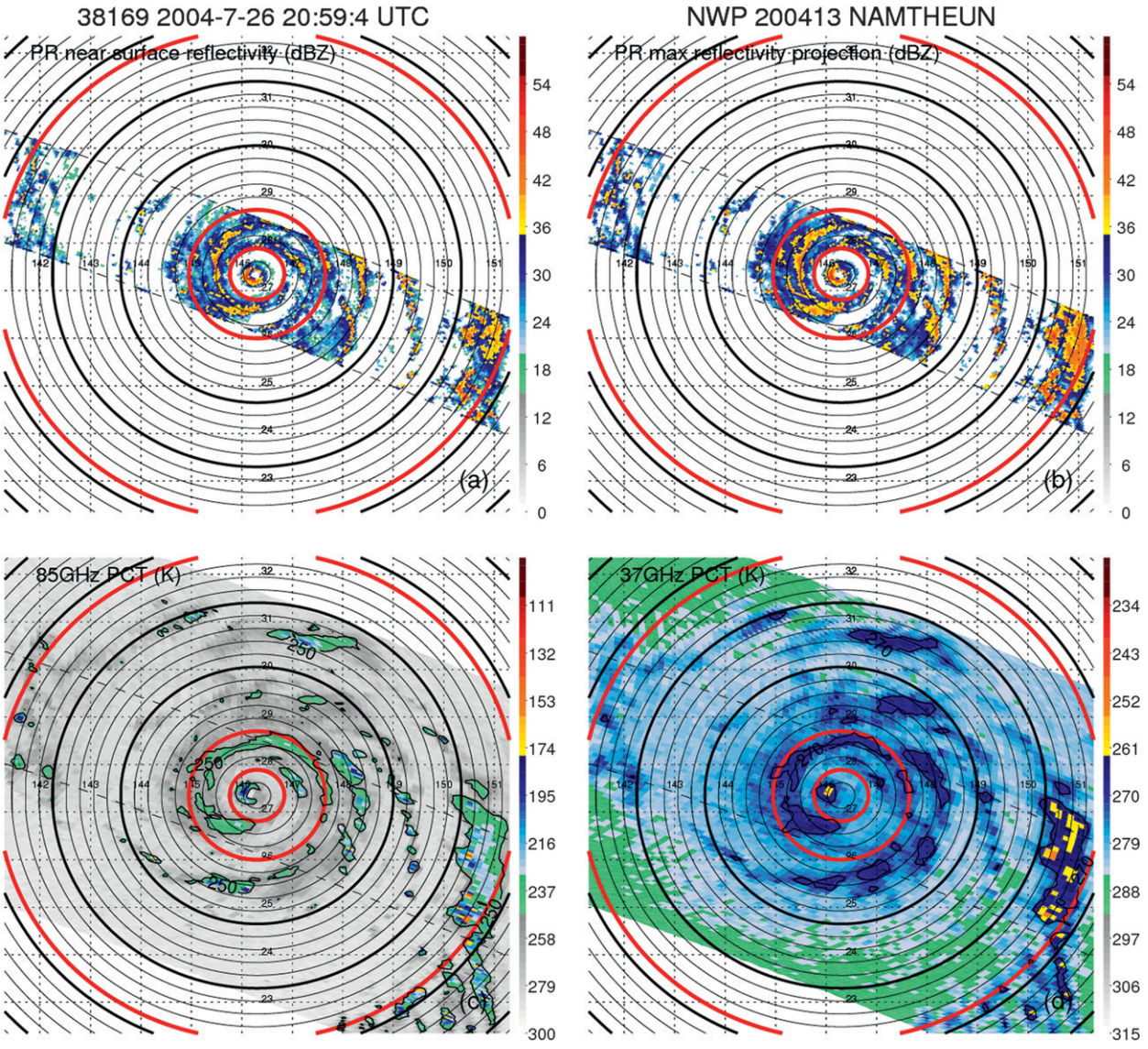

FIG. 1. Horizontal plan view of (a) PR near-surface reflectivity (dBZ), (b) PR maximum reflectivity projection (dBZ), (c) 85-GHz PCT (K), and (d) 37-GHz PCT (K) observed by TRMM for Typhoon Namtheun in the northwest Pacific basin at 2100 UTC 26 Jul 2004. The 270-K contour of 37-GHz PCT and 250-K contour of 85-GHz PCT are indicated in (c) and (d), respectively. The dashed line in (a)–(d) is the edge of the PR swath. Thin gray circles represent 30-km increments radially outward from the TC center and thick black circles represent 150-km increments radially outward from the TC center. Red circles indicate the outer edges of the IC, IB, and OB boundaries.

interpolated from the best track database, which is an archived 6-h postanalysis product from the National Hurricane Center (NHC) for TCs in the North Atlantic and eastern North Pacific basins and from the Joint Typhoon Warning Center (JTWC) for TCs in other basins. The basic size criterion of TCPFs is at minimum four pixels for PR swath features (RPFs) and one pixel for TMI swath features (TTPFs).

A series of storm parameters are calculated from the best track information, including the land/ocean flag of the TC center at the time of TRMM observations and 6, 12, 18, and 24 h in the future, the storm 24-h future intensity change, and the current and 6-, 12-, 18-, and 24-h future flag of the extratropical cyclone (EC). The EC flag is from best track data. The level-2 TRMM TCPF data also include the statistical parameters from measurements and retrievals from TRMM TMI, PR, VIRS, and LIS. Specific details of parameters available in each TCPF in level-2 data and collocation methods can be found in Liu et al. (2008) and Jiang et al. (2011). The convective intensity proxies used in this study are selected from TCPF level-2 statistical parameters (see section 2d).

TABLE 1. The mean and standard deviation radial extent of each TC region.

Radii	Mean (km)	Std dev (km)
IC	82	18
IB	162	27
OB	502	129

TABLE 2. Excerpt of RPF and TTPF descriptions from Jiang et al. (2011).

	Acronyms	Definitions	Criteria
Precipitation Features	RPF	PR feature in PR swath	2A25 rainfall rate >0
	TTPF	TMI feature in TMI swath	2A12 rainfall rate >0

c. Selection of TRMM overpasses and TCPFs

In this study, the 11-yr TRMM TCPF database is used to analyze TCs based on precipitation features. Using the recorded IC, IB, and OB radii (see section 2a) for each satellite TC overpass, TCPFs are assigned to the TC region in which they occur. If a feature crosses one regional boundary (two regional boundaries), then it is split into two (three) features. Features are included only if both the parent TC center and the feature center are over ocean. As mentioned in section 2a, more than 12 000 TRMM TC overpasses from 940 TCs during 1998–2008 are manually processed to separate IC, IB, and OB regions. Because of the limited swath width of TRMM TMI and PR, not all TRMM TC overpasses captured the storm or individual regions in full. To ensure a quality sample, if the instrument (either PR or TMI) captured a TC region (IC, IB, or OB) less than a percentage threshold, the sample is removed. The TMI swath must have observed the IC (IB, OB) region at 100% (100%, 60%) for IC (IB, OB) TTPFs to be used. The PR swath must have observed the IC (IB, OB) region at 80% (70%, 30%) for IC (IB, OB) RPFs to be used. The approximate capture percentages are estimated subjectively by visual inspection. After applying for these restrictions, the total number of TTPFs (RPFs) is 50 923 (77 044). There are a lot of small PFs in the sample. To concentrate our statistics on large PFs only, a further size restriction is applied for both TTPFs and RPFs. That is, only large PFs with raining area $\geq$1000 km^2 are included. Table 3 gives the number of TTPFs and RPFs and the number of corresponding TRMM orbits and TCs for this large PF sample. The geographic distributions of the selected TRMM TMI and PR overpasses for these large PFs are given in Fig. 2.

d. Selection of TRMM parameters

Brightness temperatures at 85- and 37-GHz channels reflect the scattering of upwelled radiation by precipitation-sized frozen hydrometeors, which reduce the background brightness temperature. The PCTs at 85 and 37 GHz are defined to remove the ambiguity between low brightness temperatures due to ice scattering and due to low sea surface emissivity (Spencer et al. 1989; CZN02). Magnitudes of temperature depressions depend on ice particle number densities and size distributions (with respect to wavelength). Compared to the 85-GHz PCT, the 37-GHz PCT is more sensitive to large rather than small ice particles. Therefore, low values of minimum 85-GHz PCT tend to indicate a large ice water path while low values of minimum 37-GHz PCT tend to indicate the presence of larger ice particles. As pointed out by Mohr and Zipser (1996a,b), the 250-K, 85-GHz PCT is considered an indicator of moderate rain. Previous studies (McGaughey et al. 1996; Mohr and Zipser 1996a,b; Nesbitt and Zipser 2003) also suggested that 85-GHz PCT $<$ 225 K can be used as a convective criterion. In this study, both the minimum 85/37-GHz PCT and percentage of pixels with 85-GHz PCT $<$ 250 K and 225 K are used as convective/rainfall proxies.

The traditional method of defining deep convection from IR data is calculating the number of pixels with brightness temperatures colder than a given threshold. The major limitation of IR T_B as a convective intensity proxy is related to the cirrus contamination. Since here the PF is grouped by a PR 2A25 or TMI 2A12 near-surface rain rate greater than zero, the cirrus contamination is reduced in this study. The minimum T_{B11} here indicates how high a convective cloud can reach.

Radar reflectivity depends on hydrometeor phase and the sixth power of hydrometeor diameter for Rayleigh scattering. Reflectivity, therefore, responds preferentially to the largest particles in a sample volume. High reflectivities below the freezing level indicate a large liquid water content, while high values above the freezing level indicate supercooled liquid raindrops or large ice particles, which can only reach those altitudes by substantial updrafts. Without strong updrafts, reflectivity

TABLE 3. The number of large TTPFs and RPFs (raining area $\geq$1000 km^2) and the number of corresponding TRMM orbits and TCs for IC, IB, and OB regions, respectively.

		IC	IB	OB	Total
TTPF	No. of large PFs	3332	4615	15 464	23 411
	No. of orbits	3204	3862	5282	5532
	No. of TCs	855	869	881	900
RPF	No. of large PFs	1243	1262	7476	9981
	No. of orbits	1124	958	2690	2984
	No. of TCs	596	553	752	833

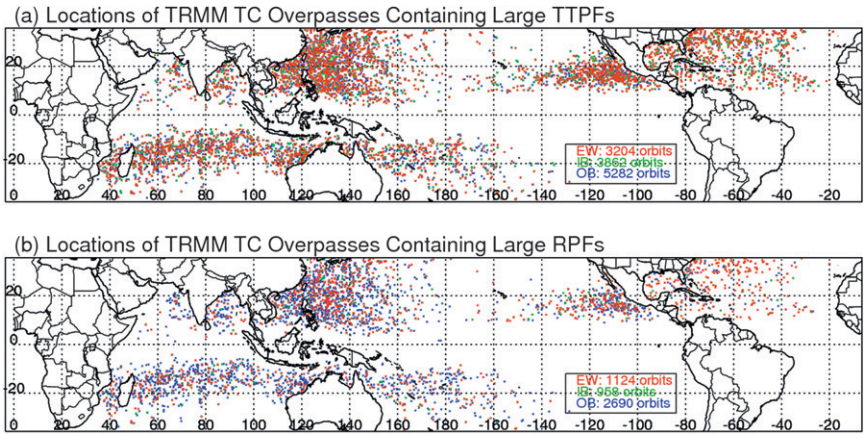

FIG. 2. Locations of TRMM TC overpasses containing (a) large TTPFs and (b) large RPFs. Overpasses containing IC, IB, and OB PFs are indicated separately by different colors. (Please see text for details about the selection of large TTPFs and RPFs.)

decreases rapidly with height above the freezing level (Zipser and LeMone 1980; Szoke et al. 1986).

Lightning requires large electric fields produced by charge separation processes within a cloud. A variety of evidence strongly suggests that a graupel–ice mechanism is dominant for electrical charge separation with sufficient magnitude to produce lightning [see reviews by Rakov and Uman (2003) and Saunders (2008)]. In this mechanism the electric charge is separated by collisions between precipitation particles (graupel) and cloud particles (small ice crystals) in the presence of supercooled liquid water (Takahashi 1978; Berdeklis and List 2001; Takahashi and Miyawaki 2002). The likelihood of strong electric fields capable of producing lightning is therefore contingent upon both the ability of an updraft core to loft liquid droplets into the mixed-phase region and the supply of liquid hydrometeors, ice crystals, and graupel. Supercooled liquid water in a hurricane, especially in the inner core region, is rare because it is quickly scavenged by the abundance of ice being horizontally redistributed about the cyclone vortex (Black and Hallett 1986). The preferred location for electrification may then be the outer rainbands of a hurricane where the environmental conditions are similar to the background non-TC environment, compared to the inner core (Molinari et al. 1994; Cecil et al. 2002).

In summary, parameters selected for the analysis of both TMI and PR swath features include total flash counts and lightning flash rate. Parameters selected for the analysis of features in the TMI swath only (TTPFs) include minimum 85/37-GHz PCT, minimum 11-μm brightness temperature T_{B11}, percentage of pixels with 85-GHz PCT $<$ 250, 225 K, 2A12 rain rate, and 2A12 raining area (e.g., PF size). Parameters selected for the analysis of features in the PR swath only (RPFs) include the 2A25 rain rate and vertical profile of maximum radar reflectivity.

3. Results and discussion

a. TMI and VIRS: Brightness temperatures and 2A12 rainfall

TTPFs (within TMI swath) are used in this section to compare convective and rainfall characteristics among IC, IB, and OB precipitation features. Figure 3 presents the cumulative distribution functions (CDFs) of minimum 85- and 37-GHz PCTs, minimum IR T_{B11} feature size (raining area), percentage of pixels with 85-GHz PCT $<$ 250 and 225 K, and TMI 2A12 conditional mean rain rate in large TTPFs in the IC, IB, and OB regions for different storm intensity categories (i.e., category-3–5 hurricane, category-1–2 hurricane, tropical storm, and tropical depression). IC features generally have colder minimum 85-GHz PCTs than IB and OB features for each storm intensity category (Fig. 3a). The median value of minimum 85-GHz PCT for IC features is lower than that for IB features, which is lower than that for OB features. As expected, the median value of minimum 85-GHz PCT for IC and IB regions decreases as the storm intensity increases. However, at the stronger end of the convective spectrum with minimum 85-GHz PCTs less than ~140 K for IC features and less than ~190 K for IB features, the gap between intensity categories narrows and eventually the order switches. There are 7.0% of IC features with minimum 85-GHz PCTs $<$ 100 K in the TS category, 3.7% in TD, 2.0% in CAT12, and only 0.8% in CAT35 categories. This implies that extremely strong

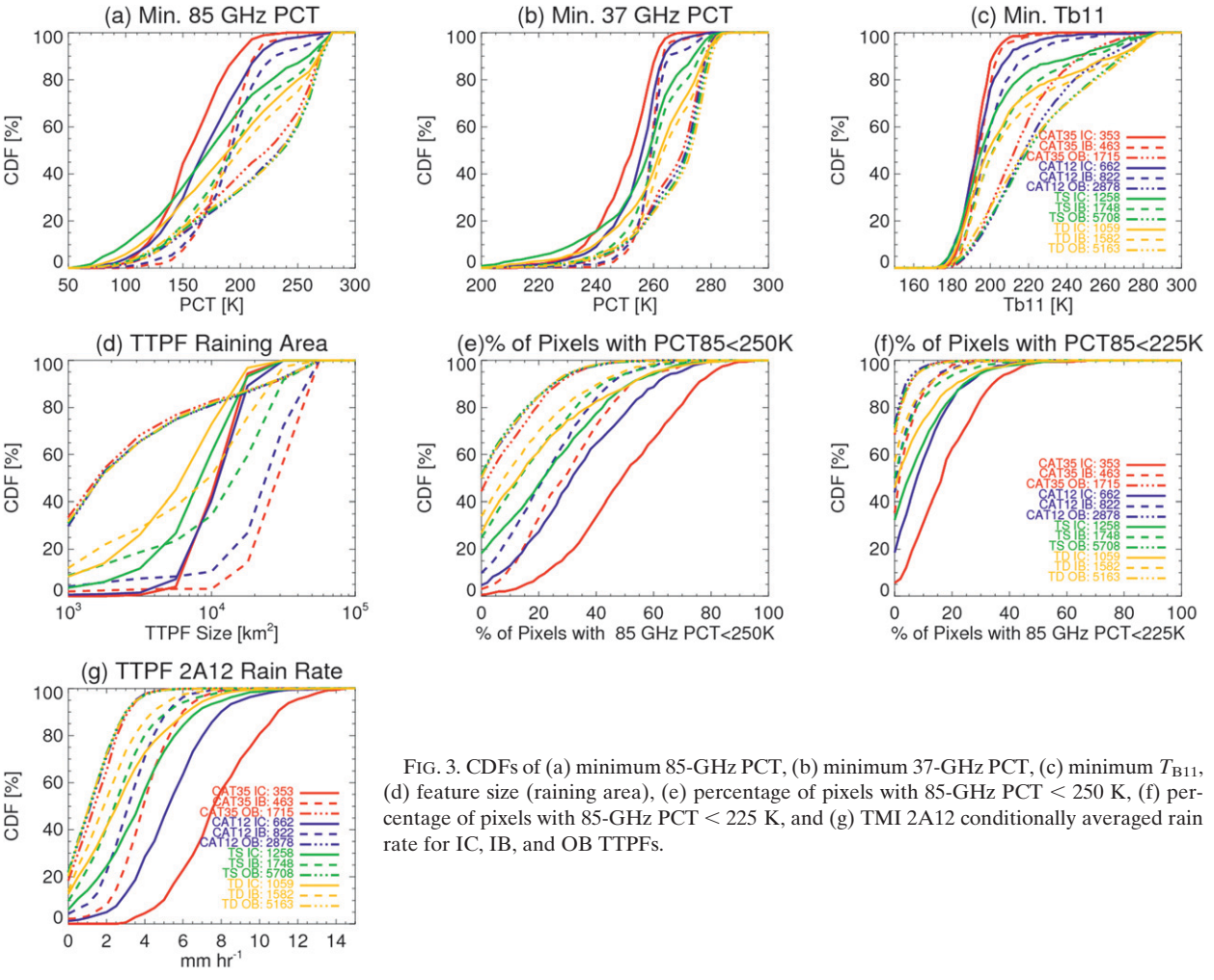

FIG. 3. CDFs of (a) minimum 85-GHz PCT, (b) minimum 37-GHz PCT, (c) minimum T_{B11}, (d) feature size (raining area), (e) percentage of pixels with 85-GHz PCT < 250 K, (f) percentage of pixels with 85-GHz PCT < 225 K, and (g) TMI 2A12 conditionally averaged rain rate for IC, IB, and OB TTPFs.

convection is more often seen in TSs and TDs than in hurricanes. Another interesting finding is that no difference in the distribution of minimum 85-GHz PCT is seen for OB features among CAT12, TS, and TD storms, although CAT35 OB features do have stronger ice scattering signatures.

Mohr and Zipser (1996a,b) used an SSM/I 85-GHz PCT of 225 K to indicate convection. On average for all storm intensity categories, approximately 43% of OB features have a minimum 85-GHz PCT falling below this threshold, as do 71% of IB features and 79% of IC features. Although CZN02 suggested that IC features usually produce strong ice scattering signatures more often than IB and OB features, they also suggested that the distributions for IB and OB features become more like those of the eyewall region after removing small features. However, Fig. 3a indicates that feature distributions in the IC region are still very different from those for IB and OB regions, even with the current 1000-km^2 size restriction.

The IB feature distribution shown in Fig. 3a may be skewed toward lower PCTs from IC contamination (even with the 1000-km^2 size restriction). Contrarily, the OB feature distribution is assuredly skewed toward higher temperatures from the high population of small (Fig. 3d) and warm features that have been acknowledged as characteristic of this region (Cecil et al. 2002; Cecil and Zipser 2002). Upon closer inspection of the stronger end of the convective spectrum, particularly with minimum 85-GHz PCT < 150 K, it is found that IC features in all TC intensity categories still have the highest percentage ($\sim$30% on average) of minimum 85-GHz PCTs below 150 K, while the percentages in IB features in TSs and TDs and OB features all TC intensity categories are comparable to each other and about a factor of 2 fewer than that in IC. The percentages of hurricane IB features with minimum 85-GHz PCTs below 150 K are the lowest, as found by CZN02, which is consistent with the lightning study by Molinari et al. (1999).

A more strict restriction is applied as follows to compare the strongest portions of the convective spectrum in features in the IC, IB, and OB regions: mesoscale convective system (MCS) TTPFs are defined for features containing a 2000-km^2 area of 85-GHz PCT less than 250 K and a 200-km^2 area less than 225 K. This follows the MCS definitions used by Mohr and Zipser (1996a) and Nesbitt et al. (2000). CDFs of minimum 85-GHz PCT in MCS TTPFs in the IC, IB, and OB regions (not shown) indicate that with minimum 85-GHz PCT $\geq$ 110 K, the OB region produces strong ice scattering slightly more often than the IC region, but much more often than the IB region. Median values are approximately 148, 152, and 175 K in OB, IC, and IB regions, respectively. However, in those parts of the plots with minimum 85-GHz PCT $\leq$ 110 K, features in the IC region produce strong ice scattering slightly more often than those in the OB region. This indicates that in the strongest convective spectrum, the convective intensity achieved in the IC region is similar to that achieved in the OB region, and is much greater than that achieved in the IB region.

Median minimum 37-GHz PCT values among TC regions have a much narrower spread (Fig. 3b). The median value of minimum 37-GHz PCT for IC features is lower than that for IB features, which is lower than that for OB features. In general, the median value of minimum 37-GHz PCT for each TC region decreases as the storm intensity increases. On average, the IC region has ~25% of its TTPFs with a minimum 37-GHz PCT below 250 K, while the IB and OB have only 10%. This implies that updrafts in the IC region are often strong enough to produce large ice hydrometeors. At the colder end of the plots, minimum 37-GHz PCT CDFs show similar characteristics to those in the distributions of minimum 85-GHz PCT (Fig. 3a) for the differences among IC, IB, and OB regions.

The minimum T_{B11} is a good indicator of cloud-top height. Figure 3c shows that the cloud-top heights of IC TTPFs are slightly higher than those in IB TTPFs, which are much higher than those in OB TTPFs for each TC intensity category. Also in each TC region, the IR cloud-top height increases as storm intensity increases. Note that IB minimum T_{B11} should be especially contaminated by IC clouds that are sloped outward.

The difference in feature size is enormous among IC, IB, and OB TTPFs (Fig. 3d). In general, the OB region has a much higher percentage of relatively small features than the IC and IB regions. The IB region has a higher percentage of large features than the IC and OB regions. Generally, the IC and IB feature size increases as storm intensity increases, but there is no difference in OB feature size for different TC intensities.

Minimum brightness temperatures are extreme values that represent just one pixel in a PF. The percentage of an area satisfying a given PCT threshold is perhaps a more appropriate convective proxy. Figures 3e,f indicate that IC TTPFs contain a larger percentage of area with 85-GHz PCT $<$ 250 and 225 K, followed by IB, then OB TTPFs for each TC intensity category. As TC intensity increases, the percentage of moderate raining area (as indicated by 85-GHz PCT $<$ 250 K) in IC, IB, and OB TTPFs also increases respectively (Fig. 3e). The relationship with storm intensity also holds for the percentage of convective area (as indicated by 85-GHz PCT $<$ 225 K) in IC features, but is not seen in IB and OB features (Fig. 3f). On average for all storm intensities, at median, one-quarter of the IC feature area is composed of pixels with 85-GHz PCT $<$ 250 K, 16% of the IB feature area, and 5% of the OB feature area. This is similar to Cecil et al. (2002), who found that on average, 45% (37%, 28%) of eyewall (inner rainband, outer rainband) pixels have 85-GHz PCT $\leq$ 250 K. In this study, it is also found that approximately 25% (35%, 61%) of IC (IB, OB) features have either no or less than 0.5% area with pixels having 85-GHz PCT $<$ 225 K. Overall, features from the IC region have a higher percentage of area that meets the convective threshold of 225 K than features from the IB and OB regions. When plotting the percentage of pixels with 85-GHz PCT $<$ 200 (not shown), the IB (IC) TTPFs produce strong ice scattering least (most) often.

Figure 3g shows the CDFs of the TMI 2A12 conditional mean rain rate for IC, IB, and OB features. IC features produce the highest conditional mean rain rates, followed by the IB and OB region features for each TC intensity category. Also, as storm intensity increases, the rain rate in IC and IB features increases accordingly. But in OB features, rain-rate distributions are almost identical among different intensity categories. This is consistent with previous studies that found that an azimuthally mean rain rate within an ~300-km radius from the storm center increases as storm intensity increases but converges for all storm intensity categories beyond an ~300-km radius (Lonfat et al. 2004; Jiang et al. 2008).

b. PR: Vertical profiles of radar reflectivity and 2A25 rainfall

RPFs (within PR swath) are used in this section to compare convective and rainfall characteristics among IC, IB, and OB precipitation features in different storm intensities. To compare the vertical profiles of radar reflectivity in IC, IB, and OB regions, the median and 90th percentile profiles of *maximum* radar reflectivity for large RPFs are derived from the PR swath dataset and plotted in Figs. 4a,b. From Fig. 4a, the median

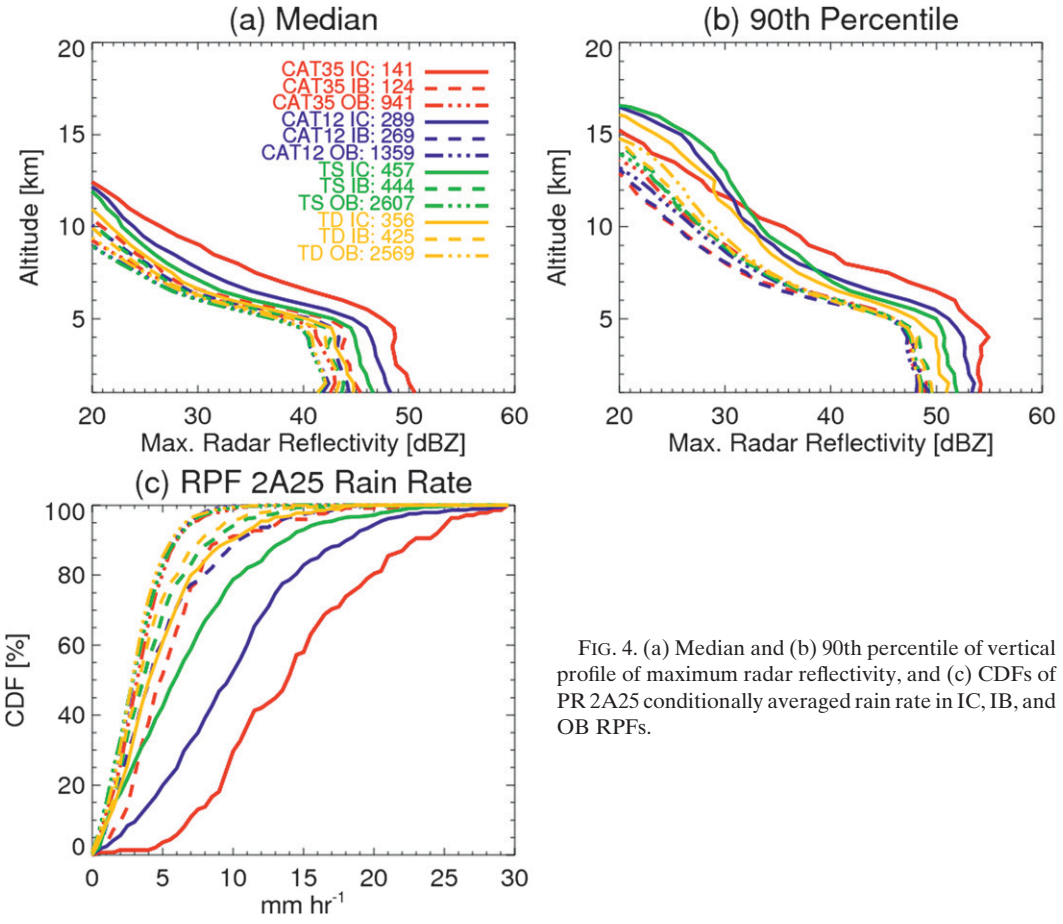

FIG. 4. (a) Median and (b) 90th percentile of vertical profile of maximum radar reflectivity, and (c) CDFs of PR 2A25 conditionally averaged rain rate in IC, IB, and OB RPFs.

heights of the 20-dBZ echoes are ~11–12, ~10, and ~9 km in IC, IB, and OB RPFs, respectively, while the median maximum near-surface reflectivities are 44–47, 43–44, and 41–43 dBZ in IC, IB, and OB RPFs, respectively. As storm intensity increases, the median profile in IC features shows larger maximum radar reflectivity values in all levels in general. But for IB and OB features, the relationship of radar reflectivity to storm intensity is not obvious. As seen in Fig. 4b, the top 10% of the 20-dBZ echo height in IC RPFs is about 1–2 km higher than that in IB and OB RPFs for each storm intensity category. However, it is interesting to see that the top 10% of the 20-dBZ echo height in IC RPFs for CAT35 hurricanes is the lowest, which is about 1.5 km lower than that for TSs and TDs. This is consistent with the CDFs of minimum 85/37-GHz PCTs shown in Fig. 3, which implies that extremely strong convection is more often seen in TSs and TDs than in hurricanes. The top 10% of the maximum near-surface radar reflectivity in IC features is still the highest for CAT35 hurricanes, followed by CAT12, TS, and TD intensities.

From both Figs. 4a,b, the IC features maintain higher altitudes at all dBZ thresholds. The IB exhibits the clearest bright band at about 5 km (Fig. 4a), which is seen by an increase in reflectivity followed by sharp decreases in reflectivity with height, and is indicative of stratiform rain. For clarification, since all the profiles in Figs. 4a,b represent the maximum reflectivity, the stratiform characteristics should be underrepresented. CZN02 separated stratiform and convective pixels in each TC region to show that stratiform precipitation is most readily found in the rainband regions and that convective precipitation most commonly occurs in the cyclone core. However, CZN02 indicated fairly similar slopes of reflectivity with height (their Fig. 4) for different TC regions, whereas here it is found that the IC samples have a slower decreased reflectivity with height compared with IB and OB samples, especially at the upper level above 10 km, suggesting stronger convective intensity in that level. Hence and Houze (2011) studied mature hurricane eyewalls from 1998 to 2007 TRMM data and found them to have the highest reflectivities, echo tops, and a relatively uniform vertical profile of reflectivity compared

TABLE 4. Number and percentage of large and all TTPFs and RPFs that contain at least one lightning flash in the IC, IB, and OB TC regions.

		IC	IB	OB	Total
TTPF	No. of large PFs	3332	4615	15 464	23 411
	No. of large PFs with lightning	383	337	1620	2340
	% of large PFs with lightning	11.5	7.3	10.5	10.0
RPF	No. of large PFs	1243	1262	7476	9981
	No. of large PFs with lightning	145	65	592	801
	% of large PFs with lightning	11.6	5.2	7.9	8.0
TTPF	No. of PFs	4701	7231	39 621	50 923
	No. of PFs with lightning	383	338	1647	2368
	% of PFs with lightning	9.4	4.7	4.2	4.7
RPF	No. of PFs	3771	6737	66 536	77 044
	No. of PFs with lightning	148	69	695	912
	% of PFs with lightning	3.9	1.0	1.0	1.2

with rainband regions. Consistent with their study, Figs. 4a,b show that both the median and 90th percentile profiles are the strongest in the IC region. However, although the median profile has higher reflectivity in the IB than the OB region, the 90th percentile profiles of the IB and OB regions are almost comparable, with the IB profile slightly stronger than the OB profile below about 8 km. For both the median and the 90th percentile profiles, the decrease immediately above the freezing level is greatest for the IB region. This is consistent with the result from passive microwave ice scattering signatures shown in Fig. 3.

Similar to the 2A12 rain-rate CDFs shown in Fig. 3g, the CDFs of the PR 2A25 conditional mean rain rate (Fig. 4c) are higher in IC features than IB features, and IB features higher than OB features for each storm intensity category. Also, as storm intensity increases, the 2A25 rain rate in IC and IB features increases accordingly. Differences between IB and OB rain rates are less pronounced in 2A25 than in 2A12. However, the magnitudes of the 2A25 rain rate are almost a factor of 2 greater than TMI 2A12 rain-rate distributions. It is likely that the differences in rain rate are inherent within the PR 2A25 and TMI 2A12 algorithms. Cecil and Wingo (2009) examined TC rain retrievals from four algorithms, including version 6 of PR 2A25 and TMI 2A12, and found that 2A25 produces the highest estimates when averaged over the 0–100-km radius because it assigns much higher rain rates, up to 100 mm h^{-1} in grid boxes with the heaviest rain. Estimates from the 2A12 algorithm were the lowest, most often assigning grid boxes to the 5 mm h^{-1} rain rate. Discrepancies were reduced when averaged farther outward and in weaker tropical cyclones. The differences can also be attributed to pixel size, as the higher resolution of PR data better represents, though not fully, the most heavily raining portions of convective cells.

c. *Lightning*

To do the lightning analysis, our first concern is how to select samples. There are two options: one is to use the large PF sample set (with 1000-km^2 size restriction; Table 3) that is used in sections 3a and 3b and then select PFs with lightning from the large PFs; the other is to select PFs with lightning from all PFs without the size restriction. Table 4 shows the number and percentage of large and all TTPFs and RPFs containing at least one flash in IC, IB, and OB regions. Slightly fewer TTPFs or RPFs with lightning are found if selecting from large PF samples. Only about 0.1% of features (28 out of 27 512 TTPFs, 111 out of 67 063 RPFs) below the 1000-km^2 size threshold have lightning, and these small features disproportionately compose the OB sample. With the 1000-km^2 size restriction, the percentage of features with lightning is substantially greater for OB than for IB. That difference goes away when the size restriction is removed. The difference in percentage of features with lightning when comparing IC with either IB or OB is much larger without the size restriction than with it. However, similar trends are seen from both the total and large PF samples: IC features tends to have a higher percentage with lightning than IB and OB features. To be consistent with previous TMI, VIRS, and PR analyses, we choose to use large PFs with the 1000-km^2 size restriction.

1) LIGHTNING VERSUS BRIGHTNESS TEMPERATURE

Large TTPFs are used in this subsection to analyze the relationship between lightning and brightness temperature in IC, IB, and OB regions. There are 383, 337, and 1620 TTPFs with lightning in the IC, IB, and OB regions, respectively (Table 4), which count for 11.5%, 7.3%, and 10.5% of the total large IC, IB, and OB features. These lightning TTPFs are from 1772 TRMM orbits (snapshots)

TABLE 5. Total lightning flash counts and flash counts per 2A12 raining area, 2A12 volumetric rain, and areas of 85-GHz PCT < 250 and 225 K in large IC, IB, and OB TTPFs for different TC intensity stages (i.e., CAT35, CAT12, TS, TD, and ALL).

		No. of large TTPFs	No. of large TTPFs with lightning	Total flash count	Flash count per 2A12 raining area (10^6 km^2)	Flash count per 2A12 volumetric rain (10^6 mm h^{-1} km^2)	Flash count per 85-GHz PCT < 250-K area (10^5 km^2)	Flash count per 85-GHz PCT < 225-K area (10^5 km^2)
CAT35	IC	353	74	415	58.1	7.0	11.3	29.8
	IB	463	21	54	2.1	0.5	0.7	3.7
	OB	1715	227	2110	18.2	6.0	8.7	51.0
CAT12	IC	662	53	256	18.6	3.2	5.3	15.7
	IB	822	49	174	4.7	1.2	1.8	9.2
	OB	2878	315	3335	18.5	6.3	9.2	49.8
TS	IC	1258	152	899	44.1	9.6	15.9	40.9
	IB	1748	159	909	18.8	5.2	8.0	28.0
	OB	5708	617	6605	23.3	8.1	11.9	55.6
TD	IC	1059	104	732	54.6	13.7	21.1	57.7
	IB	1582	108	512	16.3	5.1	7.4	27.8
	OB	5163	461	4385	17.8	6.0	8.8	37.3
ALL	IC	3332	383	2302	42.1	8.0	13.1	35.5
	IB	4615	337	1649	11.6	3.1	4.5	19.6
	OB	15 464	1620	16 435	19.9	6.8	9.9	47.6

of 676 TCs. Note that not all electrically active features are represented in the TRMM dataset, just the ones that managed to produce a flash within the relatively short 80-s TRMM LIS view time. Only PFs over ocean are included in this study.

Table 5 presents the total lightning flash counts and flash density in terms of various aspects of sample size in large IC, IB, and OB TTPFs for different storm intensity categories [i.e., CAT35, CAT12, TS, TD, and all tropical cyclones (ALL)]. The total flash count in the IC TTPFs is slightly more than that in IB TTPFs, but a factor of 7–8 less than that in the OB TTPFs for all TCs. However, it is the flash density instead of the total flash count that is a good indicator of lightning production. Figure 5 shows the flash count per 2A12 raining area, flash count per 2A12 volumetric rain, and flash counts per area of 85-GHz PCT < 250 and 225 K for large IC, IB, and OB TTPFs for different storm intensity categories. Detailed values plotted in Fig. 5 are also shown in Table 5. After normalizing the flash counts by the 2A12 raining area (Fig. 5a; column 4 in Table 5), lightning production for features in the IC region is a factor of 2–3 higher than that in the OB region for major hurricanes, tropical storms, and tropical depressions. The only exception is for category-1–2 hurricanes, where the lightning production in IC TTPFs is similar to that in OB TTPFs. The IB TTPFs produce about a factor of 4 (2) less lightning flashes per 2A12 raining area than the IC (OB) TTPFs for all TCs on average. However, this factor varies dramatically for different TC intensity groups. In major hurricanes, the lightning production in IB TTPFs is extremely low and 28 times lower than in IC TTPFs, while in other TC intensity categories, it is about a factor of 3–4 lower than that in IC TTPFs. This is the same as the results shown in Yokoyama and Takayabu (2008), who found a large rain yield per flash in the inner band, especially for stronger TCs.

The smaller lightning flash density in the IB is also consistent with the results of some other previous studies (Molinari et al. 1999; Cecil et al. 2002; Abarca et al. 2011). However, Molinari et al. (1999) found flash rate density to be 2–3 times greater for the 200–300-km-radius region (corresponding to the OB region in this study) than for the 0–60-km-radius region (corresponding to the IC region in this study). CZN02 documented similar statistics and showed that lightning production in the eyewall region is comparable to that in the outer rainband region. Since they used a sample size equal to only about 2% of the sample size used in this study, the difference might be mainly due to lack of representation of CZN02's sample. It is also possible that CZN02's sample is biased to have many more category-1–2 hurricanes than major hurricanes. The difference between this study and Molinari et al. (1999) might result from an increased ratio of in-cloud versus cloud-to-ground lightning flashes in the inner core, although we have no evidence for or against such a difference in that ratio. It could also result from the location difference. This study is for over 5000 TRMM snapshots of about 900 TCs *over ocean only*, whereas Molinari et al. was for a longer duration of observations of only 9 hurricanes *near land*.

Besides the raining area, additional parameters are used to normalize the flash counts in Fig. 5 and Table 5. The 2A12 volumetric rain (Fig. 5b; column 5 in Table 5)

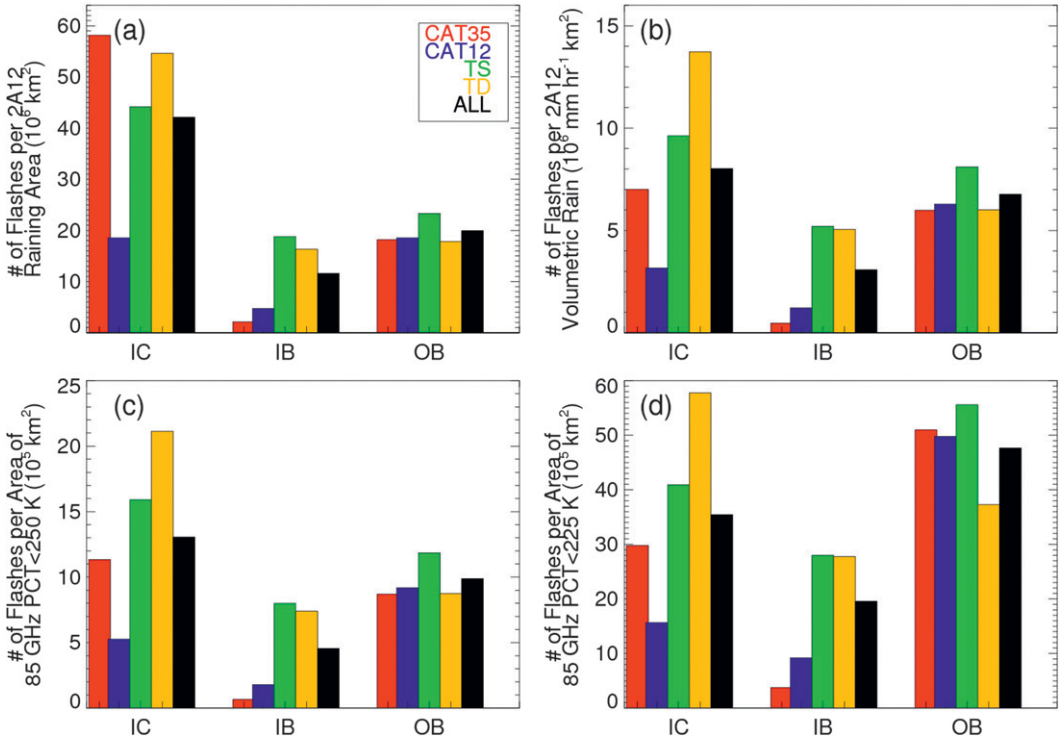

FIG. 5. Flash count per (a) 2A12 raining area, (b) 2A12 volumetric rain, (c) area of 85-GHz PCT < 250 K, and (d) area of 85-GHz PCT < 225 K for large IC, IB, and OB TTPFs for different storm intensity categories (i.e., CAT35, CAT12, TS, TD, and ALL).

combines the effects from the raining area and precipitation intensity. The area of 85-GHz PCT < 250 K (Fig. 5c; column 6 in Table 5) indicates a moderate rain rate (3 mm h^{-1}; Spencer et al. 1989), while the area of 85-GHz PCT < 225 K (Fig. 5d; column 7 in Table 5) indicates convection (Mohr and Zipser 1996a,b). The flash count in IC TTPFs per 2A12 volumetric rain (Fig. 8b; column 5 of Table 6) is slightly (a factor of 2) higher than that in OB TTPFs for major hurricanes and tropical storms (tropical depressions), but is a factor of 2 lower than that in OB TTPFs for category-1–2 hurricanes. The lightning production in IB TTPFs per 2A12 volumetric rain is about 14 (2.5, 2, and 3) times lower than that in IC TTPFs and 12 (5, 1.5, and 1.2) times lower than that in OB TTPFs for major hurricanes (category-1–2 hurricanes, tropical storms, and tropical depressions, respectively). For the weaker convective constraints (or precipitating constraints), for example, the area of 85-GHz PCT < 250 K (Fig. 5c; column 6 in Table 5), the difference in lightning productions of IC, IB, and OB features in different TC intensity stages is similar to that found by using the 2A12 raining area as the normalizing parameter. However, for the stronger convective constraints, for example, the area of 85-GHz PCT < 225 K (Fig. 5d; column 7 in Table 5), the lightning production for features in the OB region is about a factor of ~1.5–3 higher (a factor of 1.5 lower) than that in the IC region for hurricanes and tropical storms (tropical depressions). Flashes per convective area in IB TTPFs are a factor of 8 (1.7, 1.5, and 2) fewer than those in IC TTPFs for major hurricanes (category-1–2 hurricanes, tropical storms, and tropical depressions). With development from the tropical storm to hurricane to major hurricane stage, lightning becomes more and more suppressed in the inner band region. It is also noticeable from Fig. 5 that the lightning production is the lowest for category-1–2 (3–5) hurricanes in the IC (IB) TTPFs. Not much dependence on storm intensity is seen for the lightning production in OB TTPFs. This implies that the OB region is representative of the background non-TC environment as proposed by Molinari et al. (1994).

For the TTPFs with lightning, the fraction of total lightning flash counts as a function of the feature's minimum 85- and 37-GHz PCTs in the IC, IB, and OB regions is examined (Fig. 6). Lightning occurs in a wide spectrum of the TC precipitation feature's minimum PCT values (e.g., minimum 85-GHz PCT between 50 and 250 K and minimum 37-GHz PCT between 130 and 280 K). In the IC region (Fig. 6a), there are more flashes in features

TABLE 6. Total lightning flash counts and flash counts per 2A25 raining area, 2A25 volumetric rain, area of near-surface reflectivity ≥20 dBZ, and 2A23 convective area in large IC, IB, and OB RPFs for different TC intensity stages (i.e., CAT35, CAT12, TS, TD, and ALL).

		No. of large RPFs	No. of large RPFs with lightning	Total flash count	Flash count per 2A25 raining area (10^6 km^2)	Flash count per 2A25 volumetric rain (10^6 mm h^{-1} km^2)	Flash count per near-surface reflectivity ≥20-dBZ area (10^5 km^2)	Flash count per 2A23 convective area (10^5 km^2)
CAT35	IC	336	60	356	112.9	7.1	18.0	59.3
	IB	526	12	33	4.1	0.6	0.7	5.0
	OB	1174	157	1053	51.7	11.7	9.4	42.9
CAT12	IC	617	34	124	24.0	2.2	3.8	14.5
	IB	865	28	94	8.8	1.4	1.4	9.7
	OB	2456	226	1531	53.4	11.8	9.5	45.4
TS	IC	457	50	346	94.6	11.5	13.1	64.5
	IB	444	26	132	30.7	5.3	5.1	26.6
	OB	2507	205	1474	55.6	12.5	9.9	44.8
TD	IC	356	38	341	136.4	22.2	19.1	98.8
	IB	425	29	240	76.8	15.0	13.0	63.3
	OB	2569	191	1543	63.2	14.4	11.2	46.4
ALL	IC	1243	144	954	86.6	8.7	11.9	55.8
	IB	1262	65	403	28.4	4.7	4.7	27.3
	OB	7476	592	4457	56.9	12.7	10.1	45.1

having colder minimum PCT values. Flashes are mainly concentrated in IC features with minimum 85-GHz PCT ranging between 50 and 100 K and minimum 37-GHz PCT ranging between 180 and 220 K. In the IB region (Fig. 6b), the maximum flash concentration is also located in features with colder minimum PCT values (e.g., the minimum 85-GHz PCT ranging between 50 and 120 K and the minimum 37-GHz PCT ranging between 140 and 230 K). Instead, flashes in OB TTPFs (Fig. 6c) are mainly concentrated within features with moderate PCTs, for example, the minimum 85-GHz PCT ranging between 100 and 150 K and the minimum 37-GHz PCT ranging between 220 and 250 K.

Thresholds for lightning occurrence in terms of microwave brightness temperature or radar reflectivity in different weather regimes have been examined by many previous studies (Toracinta et al. 2002; Cecil et al. 2005; Xu et al. 2010; Liu et al. 2011, 2012). Their results show that thresholds vary among different weather regimes and land versus ocean. Probabilities of lightning at the given minimum 85- and 37-GHz PCTs are examined for IC, IB, and OB TTPFs in Fig. 7. It is found that the probability of lightning varies substantially among different TC regions. With the same minimum 85- and 37-GHz PCTs, OB features tend to have the highest possibility of lightning production, while the IC region features have the lowest. For example, when minimum 85-GHz PCT is near 150 K, more than 37% of OB features produce lightning, while less than 23% (14%) of IB (IC) features do. When minimum 37-GHz PCT is near 235 K, more than 70% of OB features produce lightning, while less than 42% of IC and IB features do. This is consistent with what is seen in Fig. 6 and the last column of Table 5; that is, OB features tend to have high lightning production in warmer minimum PCT ranges and produce more lightning per unit convective area than IC and IB features. Probabilities of lightning as a function of minimum 85- and 37-GHz PCTs for generic tropical oceanic TTPFs from 11 yr (1998–2009) of TRMM data are also plotted in Fig. 7 for comparison. The tropical oceanic curves are similar to OB curves, which supports the idea that the OB region is similar to the background environment (Molinari et al. 1994; Houze 2010).

2) LIGHTNING VERSUS REFLECTIVITY

Large RPFs are used in this subsection to analyze the relationship between lightning and reflectivity in IC, IB, and OB regions. As shown in Table 4, there are 145, 65, and 592 large RPFs with lightning in the IC, IB, and OB regions, respectively, as observed by the TRMM LIS in the PR swath. There are 11.6%, 5.2%, and 7.9% of large IC, IB, and OB features with lightning.

Similar to Table 5 discussed in the previous subsection, Table 6 presents the total lightning flash counts and flash density in terms of various aspects of sample size in large IC, IB, and OB RPFs for different storm intensity categories. Figure 8 shows the flash count per 2A25 raining area, flash count per 2A25 volumetric rain, flash count per area of near-surface reflectivity ≥20 dBZ, and flash count per 2A23 convective area for large IC, IB, and OB TTPFs for different storm intensity categories. These parameters are similar to the parameters used in Fig. 5 and Table 5. Detailed values plotted in Fig. 8 are also shown in Table 6.

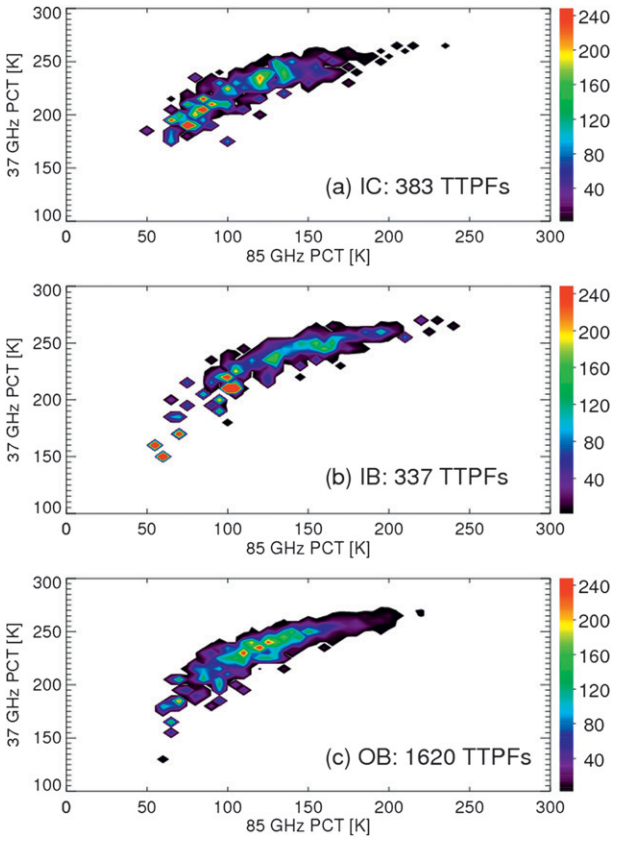

FIG. 6. Fraction of total lightning flash counts for large (a) IC, (b) IB, and (c) OB TTPFs with lightning as a function of minimum 85-GHz PCT and minimum 37-GHz PCT (in 5-K bins). The number of flashes in each PCT bin is totaled and then normalized by total flash counts in all PFs with lightning in each TC region, respectively. The unit of the color table is 10^{-4}. The sum of all values in (a)–(c) is 1.

After normalizing the flash counts by the 2A25 raining area (Fig. 8a; column 4 in Table 6), lightning production for features in the IC region is about a factor of 2–3 higher than that in the OB region for major hurricanes, tropical storms, and tropical depressions. However, for category-1–2 hurricanes, the lightning production in IC RPFs is a factor of 2 lower than that in OB RPFs. The IC and OB values were comparable to each other in the corresponding part of Table 5, for flashes per 2A12 raining area in category-1–2 hurricanes. This inconsistency might be due to 1) the truncation effect of the narrow PR swath—the sample size is down to about 100 flashes, and 2) the difference in raining area detection in the TMI 2A12 and PR 2A25 algorithms. Similar to what has been found in Fig. 8a and Table 6 for TTPFs, the IB RPFs produce about a factor of 4 (2) less lightning flashes per 2A25 raining area than the IC (OB) RPFs for all TCs on average, with the factor being much higher for major hurricanes. The lightning production in IC features per 2A25 volumetric rain amount (Fig. 8b; column 5 of Table 6) is about 1.5 times lower (2 times higher) than that in OB (IB) features for all TCs on average. The reverse of flashes per volumetric rain amount between IC and OB RPFs as compared to TTPFs is likely due to the difference between 2A25 and 2A12 rainfall retrievals. As pointed out by Cecil and Wingo (2009), version 6 of the 2A12 algorithm tends to underestimate the TC rain rate relative to version 6 of the 2A25 algorithm, especially for the inner core region. The area of near-surface reflectivity $\geq$20 dBZ per flash and 2A23 convective-certain area per flash are presented in Figs. 8c,d, and the second to last and last columns of Table 6. For both of these constraints, the lightning production of IC features is about 1.5–2 times higher than that for OB features for all TCs except for category-1–2 hurricanes in which the opposite is true. The lightning production for features in the IB region is about a factor of 2 (1.5) lower than that in the IC (OB) region on average. The difference of flashes per convective area between TTPFs (Fig. 5d; last column of Table 5) and RPFs (Fig. 8d; last column of Table 6) is likely due to the bias of the version-6 2A23 convective area identification (Yokoyama and Takayabu 2008). It might also be due to the smaller sample size of RPFs in the PR swath than TTPFs in the TMI swath.

The vertical profiles of maximum radar reflectivity for RPFs with lightning in each TC region are presented in Fig. 9. The 50th percentile of maximum radar reflectivity in the IC RPFs with lightning is even stronger than the 80th percentile and only slightly weaker than the 90th percentile in IB and OB RPFs with lightning. It shows that to produce lightning, IC features must have much stronger radar echoes than those in the IB and OB regions. Compared to Figs. 4a,b, the median profiles for features with lightning have only slightly lower values than the 90th percentile profiles for all large RPFs. The 10th percentile profiles for features with lightning even have slightly higher reflectivities than the median profiles from all large RPFs.

Figure 10 shows the probability of lightning in RPFs as a function of maximum reflectivity at 6, 8, 10, and 12 km. Thresholds required for high probability (>60%) are different for different TC regions. For example, an IC feature's maximum radar reflectivity at 6 km must reach 48 dBZ to have a lightning probability higher than 60%. However, the maximum radar reflectivity at 6 km needed for an OB (IB) feature to have the same lightning probability is only 41 (45) dBZ. The differences between IC, IB, and OB regions are slightly smaller (but still evident) when considering lightning probability as a function of reflectivity at higher altitudes. Figure 10 also indicates that features in the OB region have

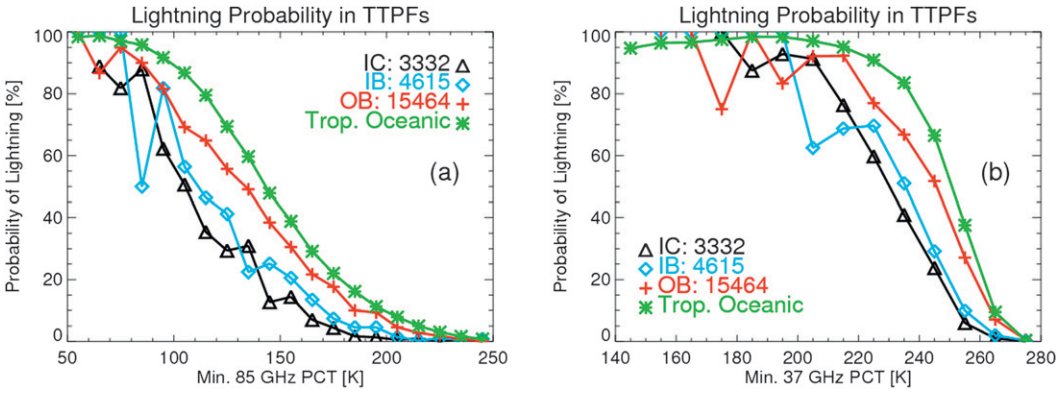

FIG. 7. Fraction of PFs with lightning as a function of the feature's (a) minimum 85-GHz PCT and (b) minimum 37-GHz PCT for large IC, IB, and OB TTPFs. The same lightning probabilities for generic tropical oceanic TTPFs are indicated for comparison (see text for details).

a higher lightning probability for almost any given reflectivity value at different altitudes than those in IC and OB regions. Probabilities of lightning as a function of maximum radar reflectivity at a given altitude for generic tropical oceanic RPFs from 11 yr (1998–2009) of TRMM data are also plotted in Fig. 10 for comparison. The tropical oceanic curves are almost overlapped with OB curves. As shown in Fig. 7, this supports the notion that the OB region is similar to the background environment (Molinari et al. 1994; Houze 2010).

The IC region's lower probability of having lightning as a function of reflectivity at a given height can partly be attributed to the TC warm core. Temperature is a more appropriate vertical coordinate for this type of analysis, as used by Liu et al. (2012). The 6-km level in the IC region might be a few degrees warmer (therefore, lower

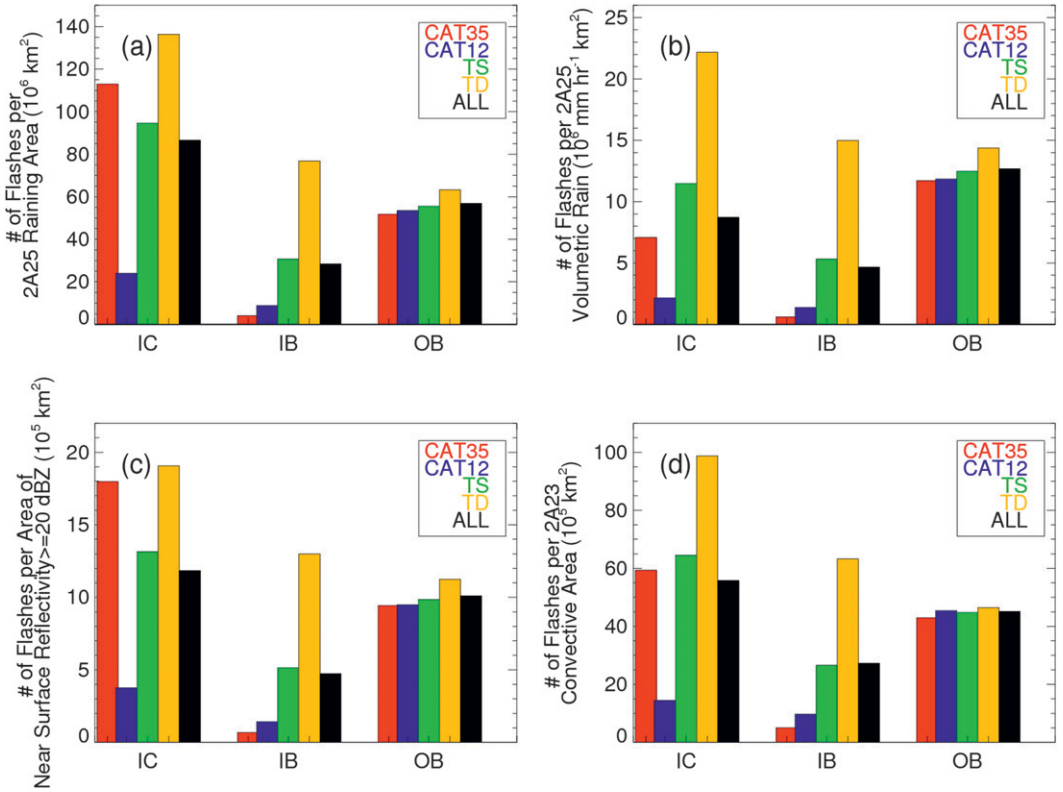

FIG. 8. Flash count per (a) 2A25 raining area, (b) 2A25 volumetric rain, (c) area of PR near-surface reflectivity ≥20 dB*Z*, and (d) 2A23 convective area for large IC, IB, and OB RPFs for different storm intensity categories.

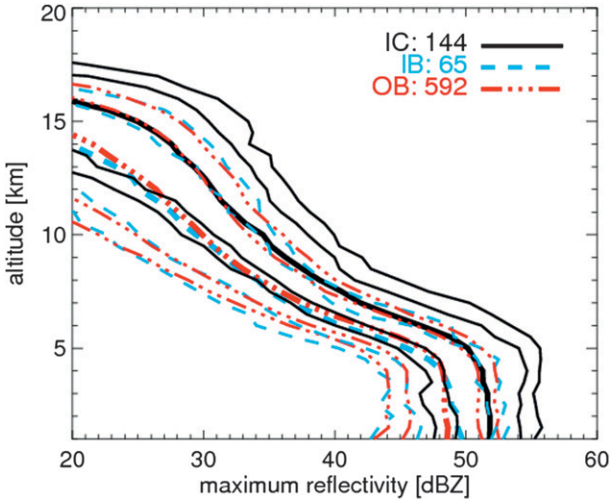

FIG. 9. The 10th, 30th, 50th, 80th, and 90th percentiles of vertical profile of maximum radar reflectivity for large IC, IB, and OB RPFs with lightning.

in the mixed-phase layer) than the 6-km level in the IB or OB region. Unfortunately, we cannot convert from altitude to temperature coordinates without reliable estimates of the vertical temperature profiles inside each TC.

4. Conclusions

Using TRMM passive microwave radiometer, IR, radar, and lightning data, this study has created a database of global TC IC, IB, and OB regions and intercompared the convective and rainfall properties of precipitation features in these distinct TC regions for different TC intensity categories.

It is found that the OB region has a much higher percentage of relatively small features than IC and IB regions. The IB region has more large features than the IC and OB regions. Strong convective signatures are more often found in the IC region, less often in the IB region, and least often in the OB region when examining features of a size greater than 1000 km^2. This is seen in the vertical profiles of maximum radar reflectivity, minimum 85/37-GHz PCT, and IR brightness temperature. However, at the very strong end of the convective spectrum, the magnitude of the ice scattering signature in OB features tends to be comparable and even stronger than that in IC features. As noted in previous studies, the IB region is dominated by stratiform rain and rather weak convection, which is also seen in this study. Therefore, the results shown here are consistent with previous studies using TRMM (CZN02; Hence and Houze 2011), aircraft radar (Szoke et al. 1986), and the updraft magnitude (Jorgensen et al. 1985; Black et al. 1996). An interesting finding of this study, by comparing IC features in different TC intensity categories, is that extremely strong convection is more often seen in TSs and TDs than in hurricanes.

By examining both TMI 2A12 and PR 2A25 rain retrievals, features in the IC region are found to have higher conditionally averaged rain rates than features in the IB and OB regions, while those of the IB region remain higher than those of the OB region. This is consistent with previous studies that found a decrease of the mean rain rate as the radial distance from the TC center increases (Rodgers et al. 2001; Lonfat et al. 2004; Jiang et al. 2008; Wingo and Cecil 2010).

For features with the 1000-km^2 size restriction, the percentage with lightning in the IC region is higher than the percentage found in the OB region, which is higher than that in the IB region. The flash density when normalized by the raining area is about 2–3 times higher in IC features than that in OB features for all TCs except category-1–2 hurricanes, in which the flash density is comparable for IC and OB features. The flash count per raining area in IB features is a factor of 2 (4) lower than that in OB (IC) features for all TC intensity categories on average. This confirms the bimodal radial distribution of flash density as suggested by Molinari et al. (1999). However, the stronger maximum in the inner core and the weaker maximum in the outer rainband found in this study are different than the results of either Molinari et al. 1999 or CZN02. When normalized by the area occupied by convection, the lightning flash density is either slightly higher in IC features than OB features or vice versa, depending on using either the RPF or TTPF dataset, although the flash density in IB features is always lower than that in IC or OB features.

The probability of a feature having lightning begins to increase as the minimum 85- (37) GHz PCT decreases below about 210 (270) K in the OB region or 180 (255) K in the IC and IB regions. Within these brightness temperatures, an OB feature is more likely to have a lightning flash than an IC or IB feature for the same given minimum of 85- or 37-GHz PCT. OB features have about a 10%–25% higher likelihood of lightning for a given maximum dBZ at 6-, 8-, 10-, and 12-km altitudes than IC and IB features. This result is consistent with the speculation of Cecil and Zipser (2002) that the OB region has more supercooled liquid water than the IC and IB regions, and is thought to be representative of the background non-TC environment (Molinari et al. 1994; Houze 2010). Since the OB region is more conducive to producing lightning for a given convective intensity (as measured by the ice scattering signature or radar reflectivity) than the IC region, combined with the fact that the flash density (as per raining area) is higher in IC features than that in OB features, it is concluded that the convective intensity in the IC region tends to be

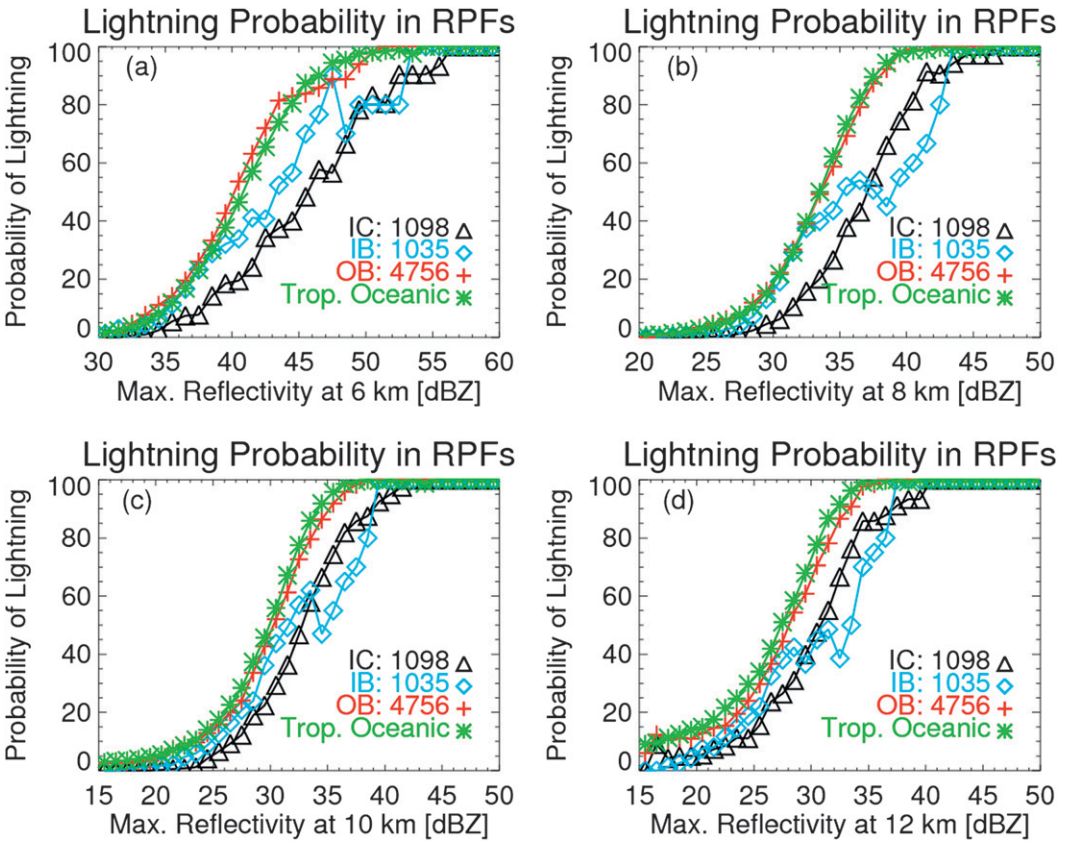

FIG. 10. Fraction of PFs with lightning as a function of the feature's maximum radar reflectivity at (a) 6, (b) 8, (c) 10, and (d) 12 km for large RPFs in IC, IB, and OB regions. The same lightning probabilities for generic tropical oceanic RPFs are indicated for comparison (see text for details).

stronger than that in the OB region. An unexplained and noteworthy exception is that the IC region of category-1–2 hurricanes has substantially less lightning than the IC region in stronger or weaker TCs.

Acknowledgments. Thanks to Drs. Ed Zipser and Steve Krueger for useful comments on this research and to Dr. Chuntao Liu for assistance with the TRMM PF database. The authors also would like to acknowledge two anonymous reviewers, whose comments helped improve the manuscript substantially. Support for this study is provided by the NASA Precipitation Measurement Mission (PMM) Grant, NASA New Investigator Program (NIP) Grant, and NASA Hurricane Science Research Program (HSRP) Grant. The authors thank Ramesh Kakar and Ming-Ying Wei (NASA headquarters) for their continued support of TRMM/PMM and hurricane sciences.

REFERENCES

Abarca, S. F., K. L. Corbosiero, and D. Vollaro, 2011: The worldwide lightning location network and convective activity in tropical cyclones. *Mon. Wea. Rev.,* **139,** 175–191.

Berdeklis, P., and R. List, 2001: The ice crystal–graupel collision charging mechanism of thunderstorm electrification. *J. Atmos. Sci.,* **58,** 2751–2770.

Black, M. L., R. W. Burpee, and F. D. Marks Jr., 1996: Vertical motion characteristics of tropical cyclones determined with airborne Doppler radial velocities. *J. Atmos. Sci.,* **53,** 1887–1909.

Black, P. G., R. W. Burpee, N. M. Dorst, and W. L. Adams, 1986: Appearance of the sea surface in tropical cyclones. *Wea. Forecasting,* **1,** 102–107.

Black, R. A., and J. Hallett, 1986: Observations of the distribution of ice in hurricanes. *J. Atmos. Sci.,* **43,** 802–822.

Boccippio, D. J., W. J. Koshak, and R. J. Blakeslee, 2002: Performance assessment of the Optical Transient Detector and Lightning Imaging Sensor. Part I: Predicted diurnal variability. *J. Atmos. Oceanic Technol.,* **19,** 1318–1332.

Cecil, D. J., and E. J. Zipser, 1999: Relationships between tropical cyclone intensity and satellite-based indicators of inner core convection: 85-GHz ice-scattering signature and lightning. *Mon. Wea. Rev.,* **127,** 103–123.

——, and ——, 2002: Reflectivity, ice scattering, and lightning characteristics of hurricane eyewalls and rainbands. Part II: Intercomparison of observations. *Mon. Wea. Rev.,* **130,** 785–801.

——, and M. Wingo, 2009: Comparison of TRMM rain-rate retrievals in tropical cyclones. *J. Meteor. Soc. Japan,* **87,** 369–380.

——, E. J. Zipser, and S. W. Nesbitt, 2002: Reflectivity, ice scattering, and lightning characteristics of hurricane eyewalls and

rainbands. Part I: Quantitative description. *Mon. Wea. Rev.,* **130,** 769–784.

——, S. J. Goodman, D. J. Boccippio, and E. J. Zipser, 2005: Three years of TRMM precipitation features. Part I: Radar, radiometric, and lightning characteristics. *Mon. Wea. Rev.,* **133,** 543–566.

Christian, H. J., R. J. Blakeslee, and S. J. Goodman, 1992: Lightning Imaging Sensor (LIS) for the Earth Observing System. NASA Tech. Memo. 4350, MSFC, Huntsville, AL, 36 pp.

——, and Coauthors, 1999: The Lightning Imaging Sensor. *Proc. 11th Int. Conf. on Atmospheric Electricity,* Huntsville, AL, National Aeronautics and Space Administration, 746–749.

DeMaria, M., R. DeMaria, J. Knaff, and D. Molenar, 2012: Tropical cyclone lightning and rapid intensity change. *Mon. Wea. Rev.,* **140,** 1828–1842.

Guimond, S. R., G. M. Heymsfield, and F. J. Turk, 2010: Multiscale observations of Hurricane Dennis (2005): The effects of hot towers on rapid intensification. *J. Atmos. Sci.,* **67,** 633–654.

Hence, D. A., and R. A. Houze Jr., 2011: Vertical structure of hurricane eyewalls as seen by the TRMM precipitation radar. *J. Atmos. Sci.,* **68,** 1637–1652.

Hendricks, E. A., M. T. Montgomery, and C. A. Davis, 2004: The role of ''vortical'' hot towers in the formation of tropical cyclone Diana (1984). *J. Atmos. Sci.,* **61,** 1209–1232.

Heymsfield, G. M., L. Tian, A. J. Heymsfield, L. Li, and S. Guimond, 2010: Characteristics of deep tropical and subtropical convection from nadir-viewing high-altitude airborne Doppler radar. *J. Atmos. Sci.,* **67,** 285–308.

Houze, R. A., Jr., 2010: Clouds in tropical cyclones. *Mon. Wea. Rev.,* **138,** 293–344.

Iguchi, T., T. Kozu, J. Kwiatkowski, R. Meneghini, J. Awaka, and K. Okamoto, 2009: Uncertainties in the rain profiling algorithm for the TRMM Precipitation Radar. *J. Meteor. Soc. Japan,* **87A,** 1–30.

Jiang, H., 2012: The relationship between tropical cyclone intensity change and the strength of inner core convection. *Mon. Wea. Rev.,* **140,** 1164–1176.

——, J. B. Halverson, J. Simpson, and E. J. Zipser, 2008: Hurricane ''rainfall potential'' derived from satellite observations aids overland rainfall prediction. *J. Appl. Meteor. Climatol.,* **47,** 944–959.

——, C. Liu, and E. J. Zipser, 2011: A TRMM-based tropical cyclone cloud and precipitation feature database. *J. Appl. Meteor. Climatol.,* **50,** 1255–1274.

Jorgensen, D. P., and M. A. LeMone, 1989: Vertical velocity characteristics of oceanic convection. *J. Atmos. Sci.,* **46,** 621–640.

——, E. J. Zipser, and M. A. LeMone, 1985: Vertical motions in intense hurricanes. *J. Atmos. Sci.,* **42,** 839–856.

Kelley, O. A., J. Stout, and J. B. Halverson, 2004: Tall precipitation cells in tropical cyclone eyewalls are associated with tropical cyclone intensification. *Geophys. Res. Lett.,* **31,** L24112, doi:10.1029/2004GL021616.

Kummerow, C., W. S. Olson, and L. Giglio, 1996: A simplified scheme for obtaining precipitation and vertical hydrometeor profiles from passive microwave sensors. *IEEE Trans. Geosci. Remote Sens.,* **34,** 1213–1232.

LeMone, M. A., and E. J. Zipser, 1980: Cumulonimbus vertical velocity events in GATE. Part I: Diameters, intensity, and mass flux distributions. *J. Atmos. Sci.,* **37,** 2444–2457.

Liu, C., E. J. Zipser, D. J. Cecil, S. W. Nesbitt, and S. Sherwood, 2008: A cloud and precipitation feature database from nine years of TRMM observations. *J. Appl. Meteor. Climatol.,* **47,** 2712–2728.

——, D. Cecil, and E. J. Zipser, 2011: Relationships between lightning flash rates and passive microwave brightness temperatures at 85 and 37 GHz over the tropics and subtropics. *J. Geophys. Res.,* **116,** D23108, doi:10.1029/2011JD016463.

——, ——, ——, K. Kronfeld, and R. Robertson, 2012: Relationships between lightning flash rates and radar reflectivity vertical structures in thunderstorms over the tropics and subtropics. *J. Geophys. Res.,* **117,** D06212, doi:10.1029/2011JD017123.

Lonfat, M., F. D. Marks, and S. S. Chen, 2004: Precipitation distribution in tropical cyclones using the tropical rainfall measuring mission (TRMM) microwave imager: A global perspective. *Mon. Wea. Rev.,* **132,** 1645–1660.

Lucas, C., E. J. Zipser, and M. A. LeMone, 1994: Vertical velocity in oceanic convection off tropical Australia. *J. Atmos. Sci.,* **51,** 3183–3193.

McGaughey, G., E. J. Zipser, R. W. Spencer, and R. E. Hood, 1996: High-resolution passive microwave observations of convective systems over the tropical Pacific Ocean. *J. Appl. Meteor.,* **35,** 1921–1947.

Mohr, K. I., and E. J. Zipser, 1996a: Defining mesoscale convective systems by their 85-GHz ice scattering signatures. *Bull. Amer. Meteor. Soc.,* **77,** 1179–1189.

——, and ——, 1996b: Mesoscale convective systems defined by their 85-GHz ice scattering signature: Size and intensity comparison over tropical oceans and continents. *Mon. Wea. Rev.,* **124,** 2417–2437.

Molinari, J., P. K. Moore, V. P. Idone, R. W. Henderson, and A. B. Saljoughy, 1994: Cloud-to-ground lightning in Hurricane Andrew. *J. Geophys. Res.,* **99,** 16 665–16 676.

——, ——, and ——, 1999: Convective structure of hurricanes as revealed by lightning locations. *Mon. Wea. Rev.,* **127,** 520–534.

Montgomery, M. T., and R. K. Smith, 2011: Paradigms for tropical-cyclone intensification. *Quart. J. Roy. Meteor. Soc.,* **137,** 1–31.

——, M. E. Nicholls, T. A. Cram, and A. B. Saunders, 2006: A vortical hot tower route to tropical cyclogenesis. *J. Atmos. Sci.,* **63,** 355–386.

Nesbitt, S. W., and E. J. Zipser, 2003: The diurnal cycle of rainfall and convective intensity according to three years of TRMM measurements. *J. Climate,* **16,** 1456–1475.

——, ——, and D. J. Cecil, 2000: A census of precipitation features in the tropics using TRMM: Radar, ice scattering, and lightning observations. *J. Climate,* **13,** 4087–4106.

Rakov, V. A., and M. A. Uman, 2003: *Lightning: Physics and Effects.* Cambridge University Press, 687 pp.

Rao, G. V., and P. D. MacArthur, 1994: The SSM/I estimated rainfall amounts of tropical cyclones and their potential in predicting the cyclone intensity changes. *Mon. Wea. Rev.,* **122,** 1568–1574.

Reasor, P. D., M. Eastin, and J. F. Gamache, 2009: Rapidly intensifying Hurricane Guillermo (1997). Part I: Low-wavenumber structure and evolution. *Mon. Wea. Rev.,* **137,** 603–631.

Rodgers, E. B., R. F. Adler, and H. F. Pierce, 2001: Contribution of tropical cyclones to the North Atlantic climatological rainfall as observed from satellites. *J. Appl. Meteor.,* **40,** 1785–1800.

Rogers, R., 2010: Convective-scale structure and evolution during a high-resolution simulation of tropical cyclone rapid intensification. *J. Atmos. Sci.,* **67,** 44–70.

Samsury, C. E., and R. E. Orville, 1994: Cloud-to-ground lightning in tropical cyclones: A study of Hurricanes Hugo (1989) and Jerry (1989). *Mon. Wea. Rev.,* **122,** 1887–1896.

Saunders, C., 2008: Charge separation mechanisms in clouds. *Space Sci. Rev.,* **137,** 335–353.

Schubert, W. H., and J. J. Hack, 1982: Inertial stability and tropical cyclone development. *J. Atmos. Sci.,* **39,** 1687–1697.

Simpson, J., R. F. Adler, and G. R. North, 1988: A proposed Tropical Rainfall Measuring Mission (TRMM) satellite. *Bull. Amer. Meteor. Soc.,* **69,** 278–295.

Spencer, R. W., H. M. Goodman, and R. E. Hood, 1989: Precipitation retrieval over land and ocean with the SSM/I: Identification and characteristics of the scattering signal. *J. Atmos. Oceanic Technol.,* **6,** 254–273.

Szoke, E. J., E. J. Zipser, and D. P. Jorgensen, 1986: A radar study of convective cells in mesoscale systems in GATE. Part I: Vertical profile statistics and comparison with hurricanes. *J. Atmos. Sci.,* **43,** 182–198.

Takahashi, T., 1978: Riming electrification as a charge generation mechanism in thunderstorms. *J. Atmos. Sci.,* **35,** 1536–1548.

——, and K. Miyawaki, 2002: Reexamination of riming electrification in a wind tunnel. *J. Atmos. Sci.,* **59,** 1018–1025.

Toracinta, E. R., D. J. Cecil, E. J. Zipser, and S. W. Nesbitt, 2002: Radar, passive microwave, and lightning characteristics of precipitating systems in the tropics. *Mon. Wea. Rev.,* **130,** 802–824.

Wingo, M. T., and D. J. Cecil, 2010: Effects of vertical wind shear on tropical cyclone precipitation. *Mon. Wea. Rev.,* **138,** 645–662.

Xu, W., E. J. Zipser, C. Liu, and H. Jiang, 2010: On the relationships between lightning frequency and thundercloud parameters of regional precipitation systems. *J. Geophys. Res.,* **115,** D12203, doi:10.1029/2009JD013385.

Yokoyama, C., and Y. N. Takayabu, 2008: A statistical study on rain characteristics of tropical cyclones using TRMM satellite data. *Mon. Wea. Rev.,* **136,** 3848–3862.

Zipser, E. J., and M. A. LeMone, 1980: Cumulonimbus vertical velocity events in GATE. Part II: Synthesis and model core structure. *J. Atmos. Sci.,* **37,** 2458–2469.